# Part II

# Underwater Robotic Vehicle Simulation

# CHAPTER VI

# Hydrodynamic Forces on a Submerged Rigid Body

## 6.1 Introduction

In Part I, dynamic simulation algorithms were developed for land-based robotic systems. In this part, simulation algorithms for underwater robotic vehicle (URV) systems are developed. The demand for such systems has risen sharply in recent years and the applications are many and varied. Industrial applications include oil exploration and rig maintenance, cable laying, surveying, and construction. Deep-sea salvage operations as evidenced by the recent Titanic expeditions are also on the rise. Scientific exploration, both geological and biological, at great ocean depths is also increasing. A recent example of this is the study of the new volcanic activity along the Juan de Fuca ridge off the coast of Oregon.

Some of the tasks can be performed by human divers, but underwater work is much more hazardous than on land. In addition, human divers are limited in the amount of time and the depth at which they can work. Much of the deep sea tasks are currently carried out with manned submarines sometimes equipped with robot manipulators that are controlled on-board. The cost of maintaining life-support suitable for the human operators within these subs, however, is quite high. As such, replacement with unmanned underwater vehicles (UUVs) is desirable, and the development of these systems has been on the rise.

One system currently under development at the Monterey Bay Aquarium Research Institute (MBARI) is a new remotely-operated vehicle (ROV), *Tiburon*, for scientific research in and exploration of the Monterey Canyon. This vehicle is designed to be operated at depths of up to 4000 meters [46]. A CAD drawing of it is shown in Figure 18. Also shown is the Schilling Titan II manipulator [47] which is mounted on the front and will be used to place and retrieve scientific equipment, acquire geological samples, and even capture live biological samples.

Another system is a six legged vehicle, called *Aquarobot* (see Figure 19), being developed by the Port and Harbor Research Institute (PHRI) at Yokosuka, Japan

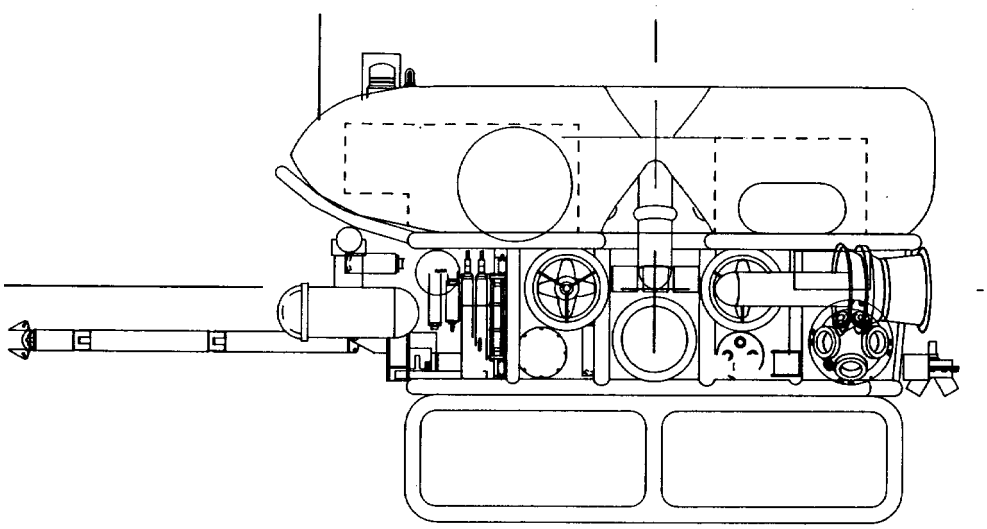

(a)

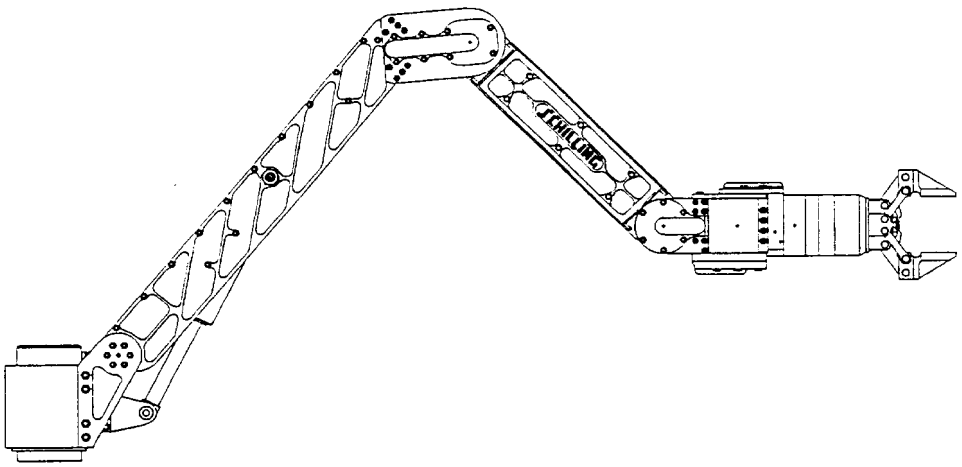

(b)

Figure 18: The MBARI UUV system: (a) *Tiburon*, and (b) the Schilling *Titan II* manipulator.

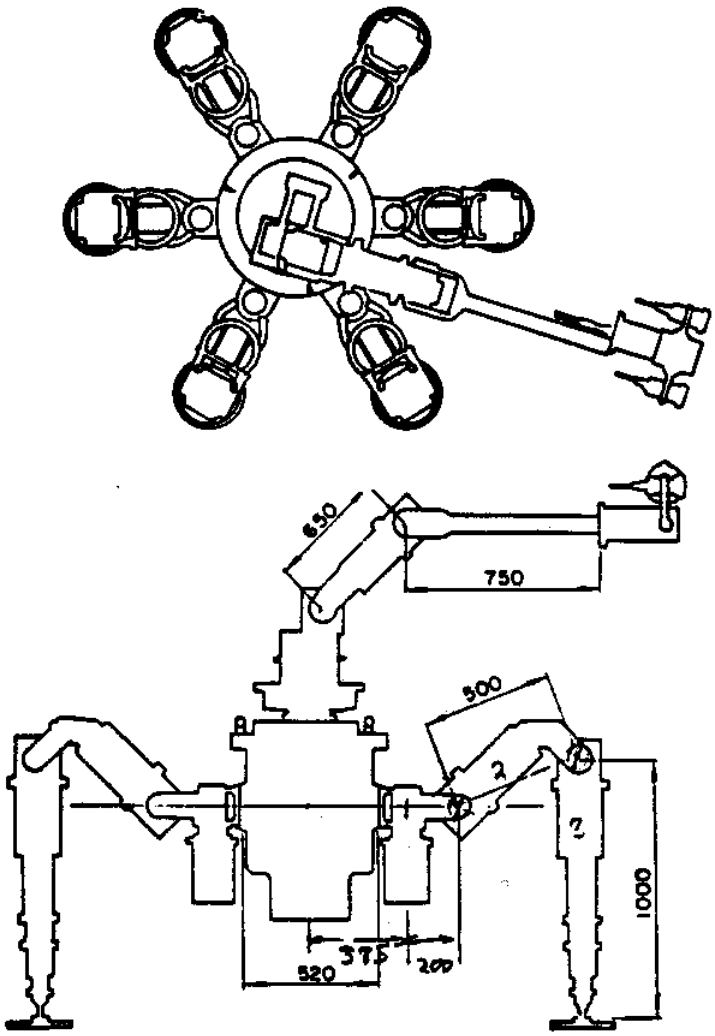


Figure 19: The *Aquarobot* hexapod (dimensions in mm) [1].

for surveying and inspection during construction of sea walls in Japan [1]. The severe tidal currents that are present increase the danger to the human divers that currently perform the tasks. The legged design was chosen to meet these needs because its ability to accurately position itself under these conditions. It can also be made smaller, weigh less, and have better mobility than other types of vehicles that move on the seabed (wheeled, tracked, and screw-driven). The primary advantage, however, is its ability to walk over uneven terrain without stirring up the sediment. This keeps visibility around the vehicle high and enables the use of underwater cameras to monitor progress.

The need for better maneuverability or agility for these and other URV systems is driving the need to perform more research in and develop more sophisticated, real-time control algorithms. Indeed, a number of papers have been written about the development of new control schemes for URVs [48, 49, 50, 51]. Some of this work addresses the problems for a single rigid body, and the hydrodynamic models used as the basis for justifying these control algorithms are simplified. This motivates the development of the best possible dynamic and hydrodynamic simulations of URVs, which has already been proven as a cost-effective development tool for equivalent land- and space-based systems. With such a tool, preliminary control algorithms can be designed and evaluated off-line without exposing expensive prototypes to completely untested algorithms that could lead to damaging instabilities. The advantage is increased when testing must proceed in the more hazardous and unpredictable underwater environments. A high fidelity simulation could also be used to evaluate the accuracy of simplified dynamics algorithms themselves which may be eventually used in model-based control algorithms.

The development and implementation of a dynamic and hydrodynamic simulation algorithm for URV systems with articulated bodies like the two described above is undertaken in this part of the dissertation. Because a significant amount of research has already been accomplished to achieve very efficient algorithms for land-based robotic vehicles, they will be used as the basis for this development. In order to use these algorithms for URV simulation, the computation of hydrodynamic forces must be accomplished first. Therefore, the purpose of this chapter is to develop detailed algorithms for computing hydrodynamic forces. Then, incorporation of these forces into an efficient dynamics simulation algorithm will be presented in Chapter 7. To complete this task, an object-oriented approach is taken to efficiently implement an algorithm that is capable of simulating URV systems with multiple serial chains (especially the two systems mentioned above) and is presented in Chapter 8.

In order to incorporate hydrodynamics into existing dynamic simulation algorithms, algorithms to compute the hydrodynamic forces on each rigid body in the system must be developed. These account for a number of additional effects when the

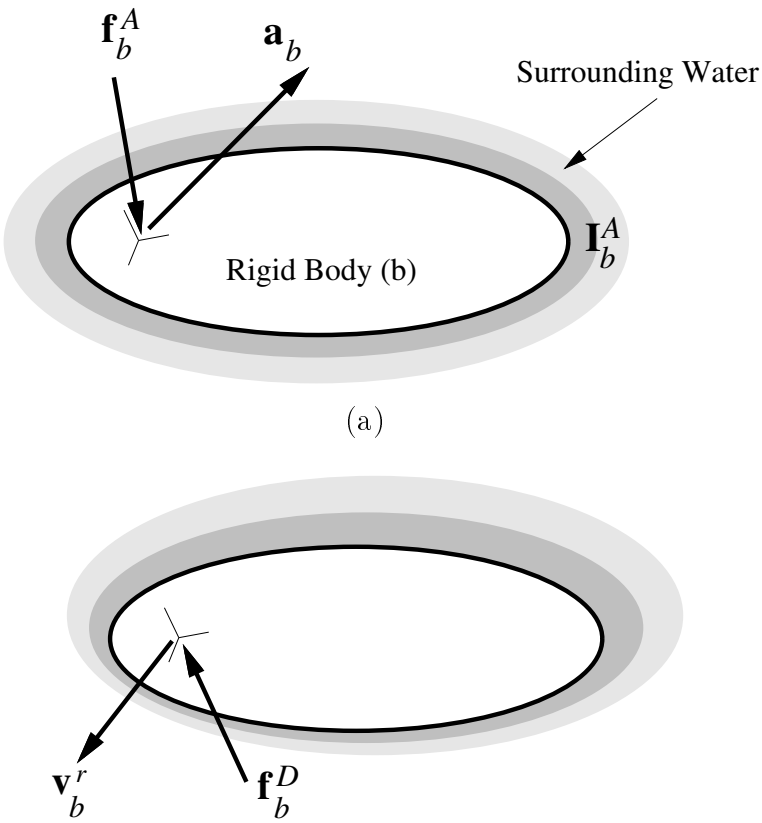


Figure 20: Hydrodynamic forces: (a) added mass and (b) drag.

motion of rigid bodies is to be simulated in an underwater environment. These forces result from incompressible fluid flow determined by the Navier-Stokes (distributed fluid-flow) equations [52]. The solution of these equations is extremely costly especially for irregularly shaped bodies undergoing general motion, and where solutions are possible, supercomputers must generally be employed.

In this chapter, "lumped" approximations to these forces are used in order to approach the desired simulation rates. To this end, work by Yuh [49] and Ioi and Itoh [50] have identified the most significant forces on a rigid body, which include added mass, viscous drag and lift, buoyancy, and fluid acceleration as illustrated in Figures 20 and 21. To facilitate incorporation into the multibody simulation algorithms in Chapter 7, particular emphasis is placed on developing notation that is consistent with the spatial notation used throughout this dissertation. In the next

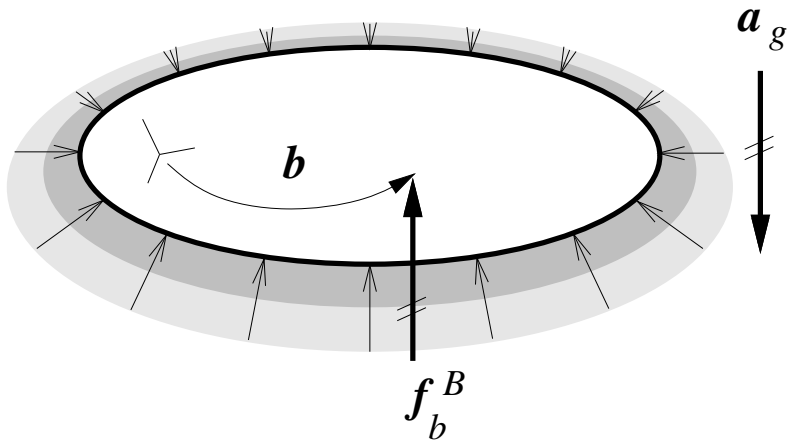


(c)

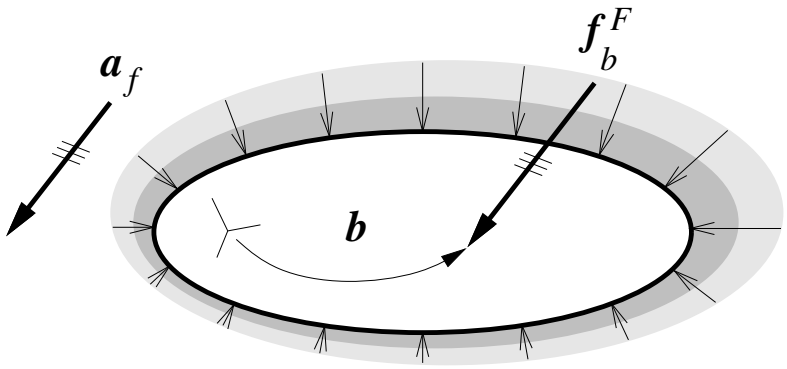


(d)

Figure 21: Hydrodynamic forces (continued): (c) buoyancy and (d) fluid acceleration.

section, the equation for the added mass force is derived. In Section 6.3, lift forces are discussed and a procedure based on strip theory is developed to compute a drag force. Due to the similarity of the resulting equations, discussion of buoyancy and forces arising from fluid acceleration are combined in Section 6.4.

## 6.2 Added Mass

To those acquainted with the dynamics of manipulators in space or on land, probably the most surprising hydrodynamic effect is the added mass force. When a body is accelerated through a fluid, some of the surrounding fluid is also accelerated with the

body. This fluid has mass/inertia properties that can be described with a $6 \times 6$ added mass matrix. A force is exerted on this surrounding fluid to achieve the acceleration, and the reaction force exerted on the body is the added mass force which is equal in magnitude and opposite in direction. The most important characteristic of this force is that it is also a function of the acceleration of the rigid body. In this section, the added mass force equation is derived using spatial notation, and is modified to a form that can be easily incorporated into robot dynamics algorithms. Then some comments about the coefficients of the added mass matrix are made.

### 6.2.1 Derivation of the Added Mass Force Equation

Newman [53] derives a set of equations to compute the added mass force that is exerted on a rigid body accelerating through an unbounded, inviscid fluid undergoing steady, irrotational flow (that is, not accelerating). This can be found by taking the derivative of the total momentum of the fluid. The results are repeated here and are translated to spatial notation. First some of Newman's notation is defined. The $ij$th element of the added mass matrix is denoted by $m_{ij}$. The body's translational velocity expressed in the body-fixed coordinate system is given by the following vector:

$$\boldsymbol{v}_b = \begin{bmatrix} U_1 \\ U_2 \\ U_3 \end{bmatrix}, \tag{6.1}$$

and a redundant notation is used to define the elements of angular velocity:

$$\boldsymbol{\omega}_b = \begin{bmatrix} U_4 \\ U_5 \\ U_6 \end{bmatrix} = \begin{bmatrix} \Omega_1 \\ \Omega_2 \\ \Omega_3 \end{bmatrix}. \tag{6.2}$$

Finally an "indicial notation" for the cross product operation is defined. The $j$th component of the result is given as follows:

$$(\boldsymbol{b} \times \boldsymbol{c})_j = \epsilon_{jkl} b_k c_l, \tag{6.3}$$

where summations are implied on the right hand side for both $k$ and $l$ from 1 to 3.

The equation to compute the three components of translational force from [53] is given by [Eq. (115), Ch. 4]:

$$F_j = -\dot{U}_i m_{ji} - \epsilon_{jkl} U_i \Omega_k m_{li}, \qquad j = 1, 2, 3, \tag{6.4}$$

where, again, summations are implied for $k$ and $l$ from 1 to 3, and for $i$ from 1 to 6. To obtain the vector equation, the summation on $i$ is made explicit and the cross

product term is isolated as follows:

$$F_j = -\sum_{i=1}^{6} m_{ji}\dot{U}_i - \sum_{i=1}^{6} U_i\left(\epsilon_{jkl}\Omega_k m_{li}\right), \quad j = 1,2,3. \tag{6.5}$$

Then, the summations are expanded and the cross products are expressed in vector notation:

$$F_j = -\left(m_{j1}\dot{U}_1 + m_{j2}\dot{U}_2 + \cdots + m_{j6}\dot{U}_6\right) - \left[U_1\left(\boldsymbol{\omega}_b \times \begin{bmatrix} m_{11} \\ m_{21} \\ m_{31} \end{bmatrix}\right)_j + U_2\left(\boldsymbol{\omega}_b \times \begin{bmatrix} m_{12} \\ m_{22} \\ m_{32} \end{bmatrix}\right)_j + \cdots + U_6\left(\boldsymbol{\omega}_b \times \begin{bmatrix} m_{16} \\ m_{26} \\ m_{36} \end{bmatrix}\right)_j\right]. \tag{6.6}$$

Finally, this is written in a form consistent with our spatial notation as follows:

$$\boldsymbol{f}_b^A = -\left[\mathbf{M}_{12} \;\; \mathbf{M}_{11}\right]\begin{bmatrix} \dot{\boldsymbol{\omega}}_b \\ \dot{\boldsymbol{v}}_b \end{bmatrix} - \tilde{\boldsymbol{\omega}}_b\left[\mathbf{M}_{12} \;\; \mathbf{M}_{11}\right]\begin{bmatrix} \boldsymbol{\omega}_b \\ \boldsymbol{v}_b \end{bmatrix}, \tag{6.7}$$

where $\boldsymbol{f}_b^A = [F_1 \; F_2 \; F_3]^T$ and the $3 \times 3$ blocks of added mass components are defined as follows:

$$\left[\mathbf{M}_{12} \;\; \mathbf{M}_{11}\right] = \left[\begin{array}{ccc|ccc} m_{14} & m_{15} & m_{16} & m_{11} & m_{12} & m_{13} \\ m_{24} & m_{25} & m_{26} & m_{21} & m_{22} & m_{23} \\ m_{34} & m_{35} & m_{36} & m_{31} & m_{32} & m_{33} \end{array}\right]. \tag{6.8}$$

Note that these blocks are "swapped" because spatial notation requires that angular components of spatial vectors appear above the translational components which is the opposite of the convention used in [53].

The equations for the moment exerted on the body due to added mass is given in [53] as follows [Eq. (116), Ch. 4]:

$$N_j = -\dot{U}_i m_{j+3,i} - \epsilon_{jkl}U_i\Omega_k m_{l+3,i} - \epsilon_{jkl}U_i U_k m_{li}, \quad j = 1,2,3, \tag{6.9}$$

where the components of moment have been specified with $N_j$ instead of the $M_j$ used in [53] to avoid confusion with mass coefficients, and the implicit summations of Eq. (6.4) also apply. This can be rewritten, as before, to highlight the summation over $i$ and the cross product operation, as follows:

$$N_j = -\sum_{i=1}^{6} m_{j+3,i}\dot{U}_i - \sum_{i=1}^{6} U_i\left(\epsilon_{jkl}\Omega_k m_{l+3,i}\right) - \sum_{i=1}^{6} U_i\left(\epsilon_{jkl}U_k m_{li}\right). \tag{6.10}$$

In Cartesian vector notation, this is written as follows:

$$N_j = -\left(m_{j+3,1}\dot{U}_1 + m_{j+3,2}\dot{U}_2 + \cdots + m_{j+3,6}\dot{U}_6\right) - \tag{6.11}$$

$$\left[U_1\left(\boldsymbol{\omega}_b \times \begin{bmatrix} m_{41} \\ m_{51} \\ m_{61} \end{bmatrix}\right)_j + U_2\left(\boldsymbol{\omega}_b \times \begin{bmatrix} m_{42} \\ m_{52} \\ m_{62} \end{bmatrix}\right)_j + \cdots + U_6\left(\boldsymbol{\omega}_b \times \begin{bmatrix} m_{46} \\ m_{56} \\ m_{66} \end{bmatrix}\right)_j\right] -$$

$$\left[U_1\left(\boldsymbol{v}_b \times \begin{bmatrix} m_{11} \\ m_{21} \\ m_{31} \end{bmatrix}\right)_j + U_2\left(\boldsymbol{v}_b \times \begin{bmatrix} m_{12} \\ m_{22} \\ m_{32} \end{bmatrix}\right)_j + \cdots + U_6\left(\boldsymbol{v}_b \times \begin{bmatrix} m_{16} \\ m_{26} \\ m_{36} \end{bmatrix}\right)_j\right],$$

where $j = 1, 2, 3$. In spatial notation, this reduces to:

$$\boldsymbol{n}_b^A = -\left[\mathbf{M}_{22} \;\; \mathbf{M}_{21}\right]\begin{bmatrix} \dot{\boldsymbol{\omega}}_b \\ \dot{\boldsymbol{v}}_b \end{bmatrix} - \tilde{\boldsymbol{\omega}}_b\left[\mathbf{M}_{22} \;\; \mathbf{M}_{21}\right]\begin{bmatrix} \boldsymbol{\omega}_b \\ \boldsymbol{v}_b \end{bmatrix} - \tilde{\boldsymbol{v}}_b\left[\mathbf{M}_{12} \;\; \mathbf{M}_{11}\right]\begin{bmatrix} \boldsymbol{\omega}_b \\ \boldsymbol{v}_b \end{bmatrix}, \tag{6.12}$$

where the added mass coefficients used in [53] are placed in the following order:

$$\left[\mathbf{M}_{22} \;\; \mathbf{M}_{21}\right] = \left[\begin{array}{ccc|ccc} m_{44} & m_{45} & m_{46} & m_{41} & m_{42} & m_{63} \\ m_{54} & m_{55} & m_{56} & m_{51} & m_{52} & m_{53} \\ m_{64} & m_{65} & m_{66} & m_{61} & m_{62} & m_{43} \end{array}\right], \tag{6.13}$$

and $\boldsymbol{n}_b^A = [N_1 \; N_2 \; N_3]^T$ is the added mass moment exerted on the rigid body.

By combining Eqs. (6.7) and (6.12), the desired equation for the added mass force is obtained in spatial notation:

$$\mathbf{f}_b^A = \begin{bmatrix} \boldsymbol{n}_b^A \\ \boldsymbol{f}_b^A \end{bmatrix} = -\mathbf{I}_b^A\begin{bmatrix} \dot{\boldsymbol{\omega}}_b \\ \dot{\boldsymbol{v}}_b \end{bmatrix} - \begin{bmatrix} \tilde{\boldsymbol{\omega}}_b & \tilde{\boldsymbol{v}}_b \\ \mathbf{0} & \tilde{\boldsymbol{\omega}}_b \end{bmatrix}\mathbf{I}_b^A\begin{bmatrix} \boldsymbol{\omega}_b \\ \boldsymbol{v}_b \end{bmatrix}, \tag{6.14}$$

where the $6 \times 6$ added mass matrix, $\mathbf{I}_b^A$, is written in terms of Newman's coefficients as:

$$\mathbf{I}_b^A = \begin{bmatrix} \mathbf{M}_{22} & \mathbf{M}_{21} \\ \mathbf{M}_{12} & \mathbf{M}_{11} \end{bmatrix}. \tag{6.15}$$

A brief discussion about their computation appears below.

In Eq. (6.14), the negative signs are needed to compute the reaction force that is exerted *onto* the rigid body, and $\boldsymbol{\omega}_b$ and $\boldsymbol{v}_b$ are the angular and translational velocities of the body, respectively. The translational acceleration term, $\dot{\boldsymbol{v}}_b$, is not

the true acceleration of the rigid body, but is rather the time derivative of $\boldsymbol{v}_b$ with respect to the body's rotating reference frame.*

Since the efficient robot simulation algorithms use the true acceleration of the body, $\boldsymbol{a}_b$, Eq. (6.14) must be modified before it can be efficiently incorporated into the algorithm. This is accomplished by using the following relationship:

$$\boldsymbol{a}_b = \dot{\boldsymbol{v}}_b + \boldsymbol{\omega}_b \times \boldsymbol{v}_b, \tag{6.16}$$

where $\dot{\boldsymbol{v}}_b$ is frequently referred to as the *rate of growth* of the acceleration vector, and $\boldsymbol{\omega}_b \times \boldsymbol{v}_b$ its *rate of transport* [55]. Substituting this into Eq (6.14) leads to the following equation for the added mass force:

$$\mathbf{f}_b^A = -\mathbf{I}_b^A \begin{bmatrix} \dot{\boldsymbol{\omega}}_b \\ \boldsymbol{a}_b \end{bmatrix} + \mathbf{I}_b^A \begin{bmatrix} \mathbf{0} \\ \boldsymbol{\omega}_b \times \boldsymbol{v}_b \end{bmatrix} - \begin{bmatrix} \tilde{\boldsymbol{\omega}}_b & \tilde{\boldsymbol{v}}_b \\ \mathbf{0} & \tilde{\boldsymbol{\omega}}_b \end{bmatrix} \mathbf{I}_b^A \begin{bmatrix} \boldsymbol{\omega}_b \\ \boldsymbol{v}_b \end{bmatrix}. \tag{6.17}$$

Now, the effects of fluid translational acceleration on the force resulting from added mass can be incorporated by replacing the translational acceleration of the rigid body with its translational acceleration *relative* to the surrounding fluid, $\boldsymbol{a}_b^r$ ([53], p. 150). This is defined as follows:

$$\boldsymbol{a}_b^r = \boldsymbol{a}_b - {}^b\boldsymbol{a}_f, \tag{6.18}$$

where ${}^b\boldsymbol{a}_f$ is the translational acceleration of the fluid expressed in the body-fixed coordinate system. Likewise, the translational velocity term is replaced with the relative translational velocity, $\boldsymbol{v}_b^r$, as follows:

$$\mathbf{f}_b^A = -\mathbf{I}_b^A \begin{bmatrix} \dot{\boldsymbol{\omega}}_b \\ \boldsymbol{a}_b \end{bmatrix} + \mathbf{I}_b^A \begin{bmatrix} \mathbf{0} \\ {}^b\boldsymbol{a}_f + \boldsymbol{\omega}_b \times \boldsymbol{v}_b^r \end{bmatrix} - \begin{bmatrix} \tilde{\boldsymbol{\omega}}_b & \tilde{\boldsymbol{v}}_b^r \\ \mathbf{0} & \tilde{\boldsymbol{\omega}}_b \end{bmatrix} \mathbf{I}_b^A \begin{bmatrix} \boldsymbol{\omega}_b \\ \boldsymbol{v}_b^r \end{bmatrix}. \tag{6.19}$$

Finally, it is desirable to write the equation in the following form which will facilitate incorporation into the robot dynamics algorithms:

$$\mathbf{f}_b^A = -\mathbf{I}_b^A \mathbf{a}_b + \boldsymbol{\beta}_b^A, \tag{6.20}$$

where

$$\boldsymbol{\beta}_b^A = \mathbf{I}_b^A \begin{bmatrix} \mathbf{0} \\ {}^b\boldsymbol{a}_f + \boldsymbol{\omega}_b \times \boldsymbol{v}_b^r \end{bmatrix} - \begin{bmatrix} \tilde{\boldsymbol{\omega}}_b & \tilde{\boldsymbol{v}}_b^r \\ \mathbf{0} & \tilde{\boldsymbol{\omega}}_b \end{bmatrix} \mathbf{I}_b^A \begin{bmatrix} \boldsymbol{\omega}_b \\ \boldsymbol{v}_b^r \end{bmatrix}, \tag{6.21}$$

which is the added mass bias force and contains all of the terms that are a function of the state and the known fluid acceleration and velocity.

Efficient computation of the bias force, assuming $\mathbf{I}_b^A$ is full, is straightforward. The first term is computed with a cross product, Cartesian vector addition, and the

*The elements of which are $\dot{u}$, $\dot{v}$, and $\dot{w}$ from [54].

equivalent of two Cartesian matrix-vector multiplies for a total of [24M, 18A]. The second term is obtained with a spatial matrix-vector multiply, three cross products, and a Cartesian vector addition for a total of [54M, 42A]. Assuming the fluid velocity and acceleration as well as the body's relative velocity have already been computed with respect to the body's coordinate system, adding the two results together is an additional spatial vector addition for a total of [78M, 66A].

### 6.2.2 Added Mass Coefficients

The added mass matrix describes the mass and inertia properties of the fluid surrounding the body that undergoes acceleration with the body. It is a distributed characteristic because the fluid nearer to the body undergoes greater acceleration than more distant fluid; therefore, the local fluid contributes more to the added mass. Various ways may be used to compute the coefficients of the added mass matrix as is shown in both Newman [53] and Sarpkaya and Isaacson [56]. One method involves the integral of the velocity potentials over the surface of the body. Another, involves an integral of the kinetic energy of the fluid within an appropriate volume surrounding the body. Both imply a dependence on the shape and motion of the body. For symmetric shapes, these equations are simplified, and for some of these shapes undergoing unseparated motion, both references, [53, 56], give tables of these coefficients. In general, however, the relationships are very complex and the coefficients can vary over time for separated motion. The determination of these coefficients has been an ongoing topic of research for over 50 years, and these authors refer to extensive lists of references.

Using lumped approximations, the fluid that is accelerated is assumed to have fixed inertia properties, and $\mathbf{I}_b^A$ is constant. As with the spatial inertia for a rigid body, this added mass matrix is symmetric and positive definite. Since this inertia is still a function of the body's surface geometry, however, there is no concept of principal axes as in rigid body analysis, along which, torque and angular momentum are collinear. In fact, with added mass, unlike the rigid body's mass, a translational force applied to a submerged rigid body can result in a non-collinear acceleration of its center of gravity as well. Consequently, the added mass matrix does not have the structure shown in Eq. (1.7) for the spatial inertia of a rigid body in space or air. For a general body shape, the matrix will be full which leads to notably different dynamic behavior.

## 6.3 Viscous Forces

When an object rotates and translates in a viscous fluid, which includes both air and water, *drag* and *lift* forces are also exerted on it. Both of these forces are a function of

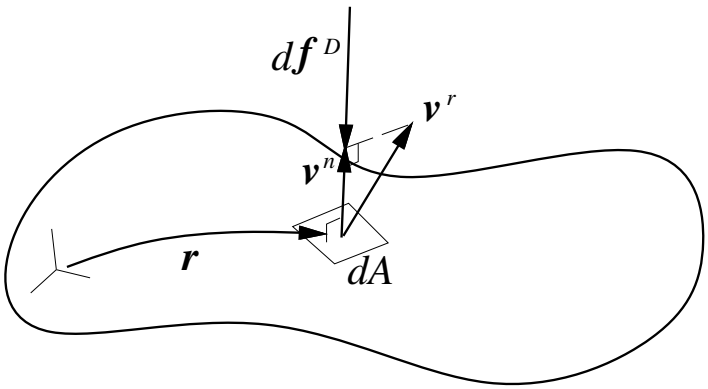


Figure 22: Drag force on a general body.

the spatial velocity of the body relative to the fluid and are discussed in this section. For simple motion, drag is a friction-like force that is in-line with the relative velocity of the body and opposite in direction; whereas, lift is a force perpendicular to the relative velocity. For most land-based robotics, the motions are slow enough and the air is thin enough that drag (air resistance) can be neglected. For underwater robotics, the fluid is significantly denser and even reasonably slow motions can result in large drag forces. This force is accentuated if the arm must move quickly to, for example, track living organisms for sample acquisition, or when operation in a strong current is desired. For the applications targeted in this development, drag is assumed to be the dominant affect and is discussed below. Lift effects including vortex shedding are discussed briefly at the end of this section.

### 6.3.1 Drag

Drag has been simplistically defined as a force proportional to the square of the relative velocity, in a direction opposite to the flow, and related by the drag coefficient, $C_D$. More generally, drag force is distributed over the surface of the body which can be decomposed into pressure (or profile) drag which is normal to the surface of the body, and shear (or skin) drag which is the tangential component. For the underwater manipulators, shear drag forces are much smaller than pressure drag forces so that the emphasis here is on the modeling of the latter. Pressure drag is a function of the components of the relative velocity between the body and the fluid that are normal to the surface of the body. From the distributed viewpoint, these velocity components are illustrated Figure 22 for an element of the surface of

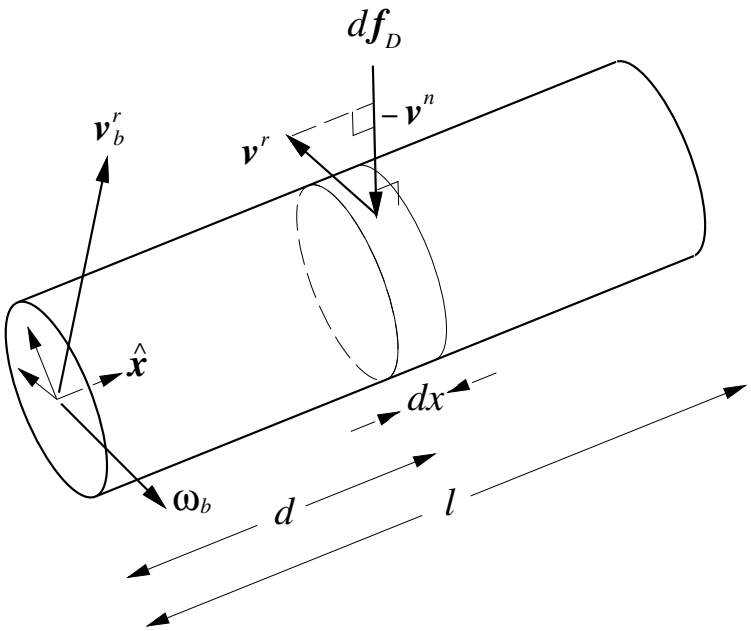


Figure 23: Drag force on a cylinder.

a general body. For each element of surface area, $dA$, on the body, the component of its relative velocity, $\boldsymbol{v}^r$, which is normal to the surface must be determined. This is labeled $\boldsymbol{v}^n$ in the figure. The partial drag force on this element, $d\boldsymbol{f}^D$, is parallel to $\boldsymbol{v}^n$ and can be computed as follows:

$$d\boldsymbol{f}^D = -0.5\rho C_D \, ||\boldsymbol{v}^n|| \, \boldsymbol{v}^n dA, \tag{6.22}$$

where $\rho$ is the fluid density, $C_D$ is the drag coefficient, and $||\boldsymbol{v}^n||$ is the magnitude of the velocity vector normal to the surface. Likewise, the partial moment about the body fixed coordinate system is given as follows:

$$d\boldsymbol{n}^D = -0.5\rho C_D \, ||\boldsymbol{v}^n|| \, (\boldsymbol{r} \times \boldsymbol{v}^n) \, dA. \tag{6.23}$$

Finally, surface integrals over the entire body are required to compute the total drag force and moment exerted on the body.

This surface integral is computationally expensive, and the drag coefficients are generally poorly known and variable. Therefore, simplifying assumptions are made to significantly reduce the amount of computation while still computing a "reasonable" drag force. The most significant assumption in this development is that the links can be approximated by cylinders or other simple symmetrical shapes. It is also desirable that one of the link's coordinate axes lies along an axis of symmetry

as shown in Figure 23 for a cylinder. This is not an unreasonable assumption since, most often, the $x$- or $y$-axis points along the length of links with revolute joints, and the $z$-axis points along prismatic links when using modified Denavit-Hartenberg parameters. Otherwise, a simple transformation can be added to the procedure to achieve this condition. The resulting procedure is based on one by Sarpkaya and Isaacson [56] to compute a drag force on a stationary cylinder arbitrarily oriented with respect to the fluid velocity. It has been extended in this section to include the effects of arbitrary translational and angular velocity of the cylinder as well.

With cylinders, strip theory is utilized to replace the surface integral with a line integral along the length of the cylinder. Therefore, the cylinder is partitioned into circular disk elements with width $dx$ as shown in the figure, and the translational velocity relative to the fluid and normal to the edge of each disk, $\boldsymbol{v}^n$, must be determined. The translational velocity of a disk relative to the fluid at a distance $d$ along the cylinder's axis (the $x$-axis in this example) is approximated, assuming the radius of the cylinder, $r$, is small compared to the length, as follows:

$$\boldsymbol{v}^r(d) \;=\; \boldsymbol{v}_b^r + \boldsymbol{\omega}_b \times \begin{bmatrix} d \\ 0 \\ 0 \end{bmatrix}. \tag{6.24}$$

where $\boldsymbol{\omega}_b$ is the angular velocity of the cylinder which is also the angular velocity relative to the fluid since it is assumed to be irrotational, and $\boldsymbol{v}_b^r$ is the translational velocity of the cylinder relative to the fluid at the body-fixed coordinate system. The relative velocity normal to this disk, $\boldsymbol{v}^n(d)$, is this vector's projection onto the $yz$-plane of the link's coordinate system which is the $y$ and $z$ components of $\boldsymbol{v}^r(d)$.

The equation to compute partial drag force exerted on the edge of this disk is obtained by modifying Eq. (6.22) for circular disks as follows:

$$d\boldsymbol{f}_b^D(d) \;=\; -0.5\rho C_D \,||\boldsymbol{v}^n(d)||\, \boldsymbol{v}^n(d)\,(2r\;dx)\,, \tag{6.25}$$

where the rightmost term inside the parentheses is the projected area of the disk normal to the fluid flow which corresponds to $dA$ in the initial equations. The equation for the corresponding partial drag moment about the body-fixed coordinate system is similarly obtained as follows:

$$d\boldsymbol{n}_b^D(d) \;=\; -0.5\rho C_D \,||\boldsymbol{v}^n(d)|| \left( \begin{bmatrix} d \\ 0 \\ 0 \end{bmatrix} \times \boldsymbol{v}^n(d) \right) 2r\;dx. \tag{6.26}$$

Eqs. (6.25) and (6.26) must then be integrated along the length of the cylinder to obtain the resultant drag force and moment as follows:

$$\boldsymbol{f}_b^D \;=\; -\rho C_D r \int_0^l ||\boldsymbol{v}^n(x)||\, \boldsymbol{v}^n(x) dx \tag{6.27}$$

$$\boldsymbol{n}_b^D = -\rho C_D r \int_0^l ||\boldsymbol{v}^n(x)|| \left( \begin{bmatrix} x \\ 0 \\ 0 \end{bmatrix} \times \boldsymbol{v}^n(x) \right) dx, \tag{6.28}$$

which correspond to the bottom and top three elements of the spatial drag force, respectively.

A numerical solution to these integrals can be obtained by using a Gauss-Legendre formula [57] which approximates the integral by computing a weighted sum of the integrand at a number of points across its range. In general, the integrand is well approximated by a polynomial, and as the number of points increases, so does the accuracy of the result. In a tradeoff between accuracy and the amount of computation required, which also increases with the number of points, a four-point version of the formula has been chosen in this research which yields an eighth order result. For an arbitrary integrand, $\boldsymbol{h}(x)$, this formula is given as follows:

$$\int_0^l \boldsymbol{h}(x)\, dx \approx l \sum_{k=1}^{4} g_k\, \boldsymbol{h}(l\, x_k), \tag{6.29}$$

where the $x_k$ are the four points at which the differential equation should be evaluated, and $g_k$ are the weights. Both of these have been determined for the four-point Gauss-Legendre (also called Gauss quadrature) method as follows:

| $k$ | $x_k$ | $g_k$ |
|---|---|---|
| 1 | 0.069431844... | 0.173927422... |
| 2 | 0.330009478... | 0.326072577... |
| 3 | 0.669990521... | 0.326072577... |
| 4 | 0.930568155... | 0.173927422... |

An off-line procedure for determining these values to the desired accuracy is also given in [57].

The result of this procedure yields zero values for the $x$-components of both the moment and force vectors. For smooth cylinders, a moment about the $x$-axis exists which would only be caused by $x$-components of angular velocity and shear drag. Therefore, a zero value in this case is consistent with the earlier assumption that shear drag is negligible. A drag force along the $x$-axis can exist, however, due to a drag force exerted on the flat ends of the cylinder to relative translational velocity along the x-axis. In this case, the $x$-component of $\boldsymbol{f}_b^D$ is simply computed as follows:

$$(f_b^D)^x = -0.5\rho C_D \left(\pi r^2\right) ||(v_b^r)^x||\, (v_b^r)^x, \tag{6.30}$$

where $(v_b^r)^x$ is the $x$-component of the link's translational velocity with respect to the fluid and $\pi r^2$ is the area projected normal to the flow in this direction.

The assumption that this component of the drag force can be computed in this manner from normal components of relative velocity for this surface while ignoring components computed for the other surfaces is consistent with the the *independence principle* [56] and the work of Chakrabarti, Tam, and Wolbert [58].

This force is determined most efficiently by computing the results of Eqs. (6.27), (6.28), and (6.30). Eq. (6.30) requires [2M, 0A] for the on-line part of the computation. The integrals in the first two equations, can be numerically determined using the Gauss-quadrature method which replaces the integral with a weighted sum of the integrand evaluated at four points over its range. The terms within both integrals require [9M, 3A] and a square root (which will be counted as a multiplication) which also includes the multiplication by the weight and the computation of $\boldsymbol{v}^r(d)$ from Eq. (6.24). Note that both of the vectors within the integrals contain one zero element. This step is performed four times, [40M, 12A], the results are added together [0M, 12A], and then multiplied by the constant outside of the integral, [4M, 0A]. Again, assuming that the relative velocity of the body has been computed, this procedure requires [46M, 24A] and the result contains five nonzero elements.

### 6.3.2 Lift and Vortex Shedding

Lift force is usually described as a force in a direction normal to the fluid flow, and is caused by non-zero net circulation of the fluid around the body [53]. It is similar to drag because it is also proportional to the square of the relative velocity. Analogous to $C_D$, the proportionality is defined by the coefficient of lift $C_L$. Like drag, this definition does not seem to be adequate for the three-dimensional derivations needed in this paper. The line integrals that are used to compute the drag force, can, in the case of general translation and rotation, result in components normal and parallel to the fluid velocity. We have called this the computation for drag forces only. Significant, steady lift forces that are distinct from the forces in that derivation are present when the body is a hydrofoil. Since the rigid bodies that make up the URVs under consideration are not foils, computation of these lift forces is omitted.

While hydrofoils with reasonable angles of attack lead to significant, steady lift forces, very large angles of attack or bluff bodies can experience significant forces due to vortex shedding. This is a second lift effect that has not been considered in this discussion. When the flow past a body becomes separated, pairs of vortices build up behind it. As the relative velocity of the body increases, these vortices continue to grow in size until instabilities cause them to alternately detach from the body. This introduces additional periodic lift forces on the body. The amplitude of this force can become large [59] if it happens to excite one of the natural frequencies of the system. For general motion of a single body, computation of these effects is extremely difficult, and precise modeling of these effects for underwater

manipulators would be even more lengthy. A straight-forward check of the Strouhal Number/Reynolds Number map, however, can yield estimates of the magnitude and frequency of this force, and can indicate if vortex shedding effects are a potential problem. Engineering solutions to reduce or even eliminate the problem using spoilers can be effective, so this phenomenon can be made small enough to ignore in most robotic applications.

## 6.4 Total Buoyancy: Buoyancy and Fluid Acceleration

Because of the similarity between buoyancy and fluid acceleration forces, they are presented together in this section. Both are translational forces as illustrated in Figure 21. They are both exerted through the center of buoyancy of the body, which is the center of volume of the body or equivalently the center of mass of the fluid that is displaced by the body. Finally, they are proportional to the mass of the fluid that is displaced by the body, $m_b^f$.

The buoyant force, $\boldsymbol{f}_b^B$, is exerted on the body in the direction opposite of gravity. This force is a result of Archimedes principle which states that a body immersed in a fluid is buoyed up with a force equal to the weight of the fluid displaced by the body. Therefore, this force is specified as follows:

$$\boldsymbol{f}_b^B = -m_b^f \, {}^b\boldsymbol{a}_g, \tag{6.31}$$

where ${}^b\boldsymbol{a}_g$ is the gravitational acceleration expressed in the body's coordinate system. In general, this acceleration is defined as follows:

$$\boldsymbol{a}_g = g \, \hat{\mathbf{z}}_e, \tag{6.32}$$

where $\hat{\mathbf{z}}_e$ is the unit vector that points "down" as is traditional in marine mechanics [54], and $g$ is the gravitational constant. This can also be thought of as the resultant force due to pressure on the surface of the body which increases with depth as illustrated by the thin arrows surrounding the body in Figure 21(c).

A similar equation was given by Newman ([53], p. 152) for the fluid acceleration force which is given as follows:

$$\boldsymbol{f}_b^F = m_b^f \, {}^b\boldsymbol{a}_f, \tag{6.33}$$

where ${}^b\boldsymbol{a}_f$ is the acceleration of the fluid also expressed in the body's coordinate system. It can also be thought of as the resultant force due to pressure that is greater at the leading edge of the body as shown in Figure 21(d). Because of the similarities, this force is often referred to as the "horizontal buoyancy" force.

For increased computational efficiency, both forces are combined as follows:

$$\boldsymbol{f}_b^{TB} = m_b^f \left( {}^b\boldsymbol{a}_f - {}^b\boldsymbol{a}_g \right), \tag{6.34}$$

and will be referred to as the "total buoyancy" force. To use this in existing robot dynamics algorithms, the equivalent spatial force exerted at the origin of the body-fixed coordinate system must be found. The resulting force is computed by the following equation:

$$\mathbf{f}_b^{TB} = \begin{bmatrix} \boldsymbol{b}_b \times \boldsymbol{f}_b^{TB} \\ \boldsymbol{f}_b^{TB} \end{bmatrix}, \tag{6.35}$$

where $\boldsymbol{b}_b$ is the vector from the body-fixed coordinate system to its center of buoyancy. With ${}^b\boldsymbol{a}_g$ and ${}^b\boldsymbol{a}_f$ already computed, the computation of this force requires [9M, 6A].

## 6.5 Summary and Conclusions

In this chapter, the most significant hydrodynamic effects present in most underwater robotic activities have been presented. Of these, computational procedures for computing added mass, drag, fluid acceleration, and buoyancy effects have been presented. Because computation of precise forces is extremely difficult and time consuming (computational fluid dynamics is a task usually relegated to supercomputers), a number of simplifying assumptions have been made. The most notable assumptions are that the fluid is irrotational and unbounded. The former is acceptable since rotation due to any vortices in the fluid are generally small compared to rotation of the body, or limited to such a small scale (as in the case of shed vortices) compared to the extent of the body as to be negligible. The exception is circular wave action in shallow depths, which is not an environment that is encountered in applications reserved for UUV systems. The unbounded assumption poses more of a problem, but for first order approximations it should generally be acceptable.

Another assumption is that the added mass matrix and drag coefficients are known and constant. In actuality, these quantities are extremely difficult to compute with a high degree of accuracy, and vary non-linearly with respect to velocity and other parameters [56]. However, we believe that over the range of operating conditions typically encountered by a UUV, these coefficients vary by only small amounts such that a constant coefficient assumption is a reasonable approach and is adequate for the purposes of the desired application. With these results, the next chapter develops a multibody dynamics algorithm and incorporates these hydrodynamic effects in order to develop a simulator for the URVs illustrated in the introduction to this chapter.